PCCP

Check for updates

Influence of the emission site on the photoelectron circular dichroism in trifluoromethyloxirane†

Kilian Fehre,[a] Florian Trinter, [ID] [ab] Nikolay M. Novikovskiy, [ID] [cd] Sven Grundmann, [ID] [a] Dimitrios Tsitsonis,[a] Sebastian Eckart, [ID] [a] Leonie Bauer,[a] Maria Hilzinger,[a] Till Jahnke,[e] Reinhard Dörner,[a] Philipp V. Demekhin [ID] [c] and Markus S. Schöffler [ID] *[a]

We report a joint experimental and theoretical study of the differential photoelectron circular dichroism (PECD) in inner-shell photoionization of uniaxially oriented trifluoromethyloxirane. By adjusting the photon energy of the circularly polarized synchrotron radiation, we address 1s-photoionization of the oxygen, different carbon, and all fluorine atoms. The photon energies were chosen such that in all cases electrons with a similar kinetic energy of about 11 eV are emitted. Employing coincident detection of electrons and fragment ions, we concentrate on identical molecular fragmentation channels for all of the electron-emitter scenarios. Thereby, we systematically examine the influence of the emission site of the photoelectron wave on the differential PECD. We observe large differences in the PECD signals. The present experimental results are supported by corresponding relaxed-core Hartree−Fock calculations.

1 Introduction

Most large molecules, including most biomolecules and the building blocks of life, are chiral.[1] Therefore, there is a great interest in the development of highly sensitive methods for chiral recognition in analytical chemistry and pharmacy. In the realm of gas-phase studies, several techniques have emerged so far, but, for example, the direct determination of the handedness of chiral molecules by Coulomb explosion imaging is currently restricted to small molecules.[2,3] In the last two decades, exploiting photoelectron circular dichroism (PECD[4]) has become a new and promising tool for the recognition of chiral molecules in the gas phase.[5–7] PECD signals are up to three orders of magnitude stronger as compared to those of the closely related conventional circular dichroism. While the latter

one relies on a scalar observable, namely the helicity-dependent difference in the absorption probability of circularly polarized light by chiral molecules, a vectorial observable is investigated in the case of PECD (emerging from randomly oriented molecules), namely the helicity-dependent emission probability of the photoelectron as a function of its emission angle with respect to the light propagation direction. Due to the much larger signal strength, PECD is especially suitable for accurate examination of dilute gas-phase samples or samples with small enantiomeric excesses.[8,9]

PECD is highly sensitive to the molecular structure,[10] spatial orientation of the molecule,[11–13] vibrational[14–16] and conformational states,[17–19] and to dimerization.[20] The dynamics of chiral molecules was also investigated in time-resolved measurements.[21–23] A further important advantage of PECD is its insensitivity to fluctuations in the target density or the photon flux. The effect of possible fluctuations is eliminated by normalization for differential signals.[24] Besides on structural properties of the molecule, PECD also depends on many parameters, such as the photoelectron energy,[25,26] possible intermediate states populated during the ionization process,[27,28] or molecular resonances.[29,30] In addition, the orbital from which the photoelectron is ionized influences the PECD signal.[26,31,32]

For randomly oriented molecules in the gas phase, PECD is typically on the order of a few percent. Its strength, however, can already be increased about ten times when fixing one

[a] *Institut für Kernphysik, Goethe-Universität Frankfurt, Max-von-Laue-Straße 1, 60438 Frankfurt am Main, Germany. E-mail: fehre@atom.uni-frankfurt.de, schoeffler@atom.uni-frankfurt.de*

[b] *Molecular Physics, Fritz-Haber-Institut der Max-Planck-Gesellschaft, Faradayweg 4-6, 14195 Berlin, Germany*
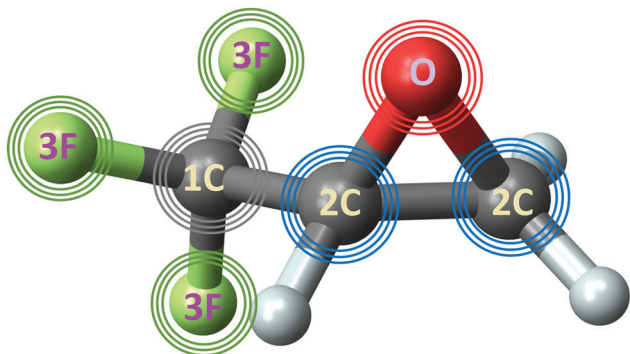
[c] *Institut für Physik und CINSaT, Universität Kassel, Heinrich-Plett-Straße 40, 34132 Kassel, Germany. E-mail: demekhin@physik.uni-kassel.de*

[d] *Institute of Physics, Southern Federal University, 344090 Rostov-on-Don, Russia*

[e] *European XFEL GmbH, Holzkoppel 4, 22869 Schenefeld, Germany*

† Electronic supplementary information (ESI) available. See DOI: https://doi.org/10.1039/d2cp00143h

This journal is © the Owner Societies 2022

Phys. Chem. Chem. Phys., 2022, **24**, 13597–13604 | 13597

Fig. 1 Structure of R-TFMOx. Photoelectrons emitted from the 1s-orbitals of the oxygen (red), fluorine (green), and carbon (grey) atoms are sketched by respectively coloured circles (waves) originating from those atoms. The photon energies were adjusted such that the photoelectron kinetic energy was 11 eV for the respective emitter. Owing to a large chemical shift in the CF$_3$-group, the 1s-photoelectron signal from this carbon (waves in grey) was distinguished from those originating from the two carbons in the oxirane ring (waves in blue).

molecular orientation axis in space.[11,12] Moreover, for distinct molecular orientations, the normalized chiral asymmetry can exceed 50%,[13] and such giant differential PECD of fully fixed-in-space chiral molecules provides higher sensitivity in the enantiomeric-excess determination. In our previous work, ref. 12, we reported on PECD as a function of a molecular fragmentation direction, *i.e.*, on PECD of uniaxially oriented tri-fluoromethyloxirane (C$_3$H$_3$F$_3$O, TFMOx). For O 1s-photoionization of TFMOx, we studied the energy dependence of the chiral asymmetry and its sensitivity to the molecular configuration, as compared to its close relative methyloxirane (C$_3$H$_6$O).

In the present work, we continue our investigation of such differential PECD in the inner-shell photoionization of uniaxially oriented TFMOx and study its emission-site sensitivity for a fixed photoelectron kinetic energy of 11 eV. To this end, we compare differential PECDs for O 1s-photoionization of TFMOx[12] with that obtained for the 1s-photoionization of different carbon and all fluorine atoms in the molecule. The structure of TFMOx and the processes studied in the present work are schematically visualized in Fig. 1.

2 Experiment and theory

The experimental data for the O 1s-photoionization of TFMOx were recorded during the same experimental campaign as the data reported in ref. 12 at Synchrotron SOLEIL (Saint-Aubin, France) at beamline SEXTANTS. The respective experimental details can be found therein.[12] The experiment providing the results for the F 1s-photoionization and the two cases of C 1s-photoionization was conducted at PETRA III, DESY (Hamburg, Germany) at beamline P04.[33] To ensure equal experimental conditions for the two light helicities, we switched every two hours between circular left and circular right polarization. The R-TFMOx was brought into vacuum by supersonic expansion, expanding through a 60 μm nozzle. Subsequently, the gas jet was skimmed two times and crossed at right angle with the

synchrotron light. About 95% of the non-used gas was recycled multiple times, using a closed-loop approach.[34] The sample had an enantiomeric excess of 95% and a chemical purity of > 98%.[12] In a coincident measurement, the photoelectron and the ionic fragments were recorded with 4π solid angle using the permanent COLTRIMS[35–37] end-station at beamline P04 at DESY. The ion arm of the spectrometer consisted of a mesh-free homogeneous 17 cm long acceleration region guiding the ionic fragments onto a hexagonal delay-line detector with an active diameter of 75 mm. The electron arm was built in a time-focusing geometry,[38] with 4.5 cm acceleration and 7.5 cm drift length, not being separated by a mesh. The electric field was set to 130 V cm^{-1} in order to separate the different fragmentation channels already in the photoion–photoion coincidence spectrum. With this voltage, electrons with kinetic energies up to 15 eV were captured with 4π solid angle without the need of applying a magnetic confinement field. Also, all ionic fragments considered in this manuscript were captured with full solid angle of 4π. From the particle's time-of-flight, its momentum along the direction of the electric field as well as the mass-to-charge ratio in case of ions can be deduced, based on the spectrometer geometry and field strength. From the impact position on the detector, the transverse momentum is derived. The electron-energy resolution in the detector plane was sufficient to resolve the energy difference between the C 1s-photoelectrons of the CF$_3$-group and of the two carbon atoms in the oxirane ring; the energy resolution in the third dimension (typically referred to as the "time-of-flight" direction) was not sufficient for that purpose due to the high electric field in the spectrometer, required to separate the different ion masses (m/q), *i.e.*, fragmentation channels. Therefore, only electron momenta restricted to the detector plane with $|p_z| < 0.35$ a.u. were considered in the analysis. So-called funnel microchannel plates (MCPs) were used on the ion detector to increase the coincident detection efficiency[39] by a factor of 2 for the two-body breakup. We first performed calibration measurements for both the electron and ion arms of the spectrometer using the known Ar 2p- and N$_2$ 1s-photoionizations. Thereafter, the photon energies were tuned such that photoelectrons of $E_e = E_\gamma - E_b = 11$ eV were emitted. Given the chemical shift of the different sites, this corresponded to photon energies of $E_\gamma = 706$ eV, 550 eV, 310 eV, and 305 eV for the F, O, C (trifluoromethyl group), and the C (oxirane ring) atoms.

A typical approach to separate the real signal from false coincidences and background is to check whether the measured particles comply with momentum conservation. Since breakup channels with undetected (neutral) particles were used for the analysis in order to gather sufficient statistics, the background suppression *via* this approach was not as effective as for breakup channels where all fragments are detected. Instead, we used several, less strict gates to successfully suppress the background from desired fragmentation channels. The first gate selected the time-of-flight combinations in the photoion–photoion coincidence spectrum to have ions with the proper m/q ratio. In the second step, the momentum of each of the two measured ionic fragments was restricted to (85–145 a.u.)/(75–145 a.u.), (80–130 a.u.)/(105–155 a.u.), (85–145 a.u.)/(75–145 a.u.), and (75–165 a.u.)/(50–175 a.u.),

13598 | *Phys. Chem. Chem. Phys.*, 2022, **24**, 13597–13604

This journal is © the Owner Societies 2022

respectively for the light/heavy charged fragment of the fragmentation channels $CF_3^+(m/q = 69)$–$C_2H_2^+(m/q = 26)$, $CF_3^+(m/q = 69)$–$COH^+(m/q = 29)$, $CF_2^+(m/q = 50)$–$C_2H_2^+(m/q = 26)$, and $CF_2^+(m/q = 50)$–$COH^+(m/q = 29)$. And third, the magnitude of the calculated sum momentum was selected to be smaller than 60 a.u. Assuming the validity of the axial-recoil approximation,[40] the ionic fragments' momenta are directly correlated with the orientation of a molecule in space at the instant of ionization. We used the momentum vector of the $CF_{2,3}^+$ fragment to define the angle β between the molecular breakup axis and the light propagation direction.

The calculations of the angle-resolved 1s-photoionization of all fluorine and carbon atoms in TFMOx were performed similarly to those reported in our previous study of the O 1s-photoionization of this molecule.[12] Briefly, the calculations were performed at the equilibrium internuclear geometry of the electronic ground state of the neutral molecule in the relaxed-core Hartree–Fock approximation by the Single Center (SC) method.[41,42] The SC expansions were restricted by the angular momenta and their projections ℓm of 79 and 29, respectively, for the occupied and continuum orbitals. In the experiment, the asymptotic momenta of the detected ions are measured, and it is not straightforward to assign the emission directions of the fragments to the orientation of a particular molecular orientation axis at the instant of the photoionization. This is because for large fragments, whose centers of mass do not coincide with their centers of charge, rotations of the fragments with respect to each other take place during the complex fragmentation dynamics. Therefore, the molecular orientation axis at the instant of the photoionization process was used as a free parameter when comparing the measured data to the calculations.[11,12] At first, the angle-resolved photoionization spectra were generated for different spatial orientations of the assumed fragmentation axis with respect to the light propagation direction, which are defined by the two Euler angles α_o and β_o. Since only one fragmentation direction is detected in the experiment, the computed spectra were then numerically integrated over the orientation angle α_o to simulate a uniaxially oriented molecule. In addition, the spectra computed for individual fluorine atoms and, separately, for the two carbon atoms in the oxirane ring were averaged to simulate the experimentally unresolved PECD landscapes. Starting with an assumption based on the axial-recoil approximation,[40] we searched for the optimal choice of the assumed molecular fragmentation axis, which provides the best visual correspondence[11] between the computed and measured differential PECD.

3 Results and discussion

As discussed above, we studied the 1s-photoionization of all heavy atoms in R-TFMOx (indicated by coloured circles in Fig. 1). The K-shell ionization energies of different chemical elements (F, O, and C) differ by several hundreds of electron volts and, thus, can be addressed unambiguously. A very small difference between the 1s-binding energies of the three fluorine atoms (about 90 meV), Auger decay lifetime broadenings, very rich vibrational structures of the respective photoelectron lines, and the limited electron-energy resolution, all together, do not allow for resolving the respective photoelectrons in our experiment. We thus considered the unresolved photoelectron spectra of all three fluorine atoms (hereafter referred to as 3F). The 1s-binding energy of the carbon atom in the CF_3-group is about 5 eV larger than that of the two carbon atoms in the oxirane ring, which allows to unambiguously resolve its 1s-photoelectrons (1C). On the contrary, the 1s-binding energies of the two carbon atoms in the oxirane ring differ only by a few 100 meV and, owing to the same reasons as for the fluorine atoms, could thus not be resolved in the present experiment (2C).

At first, the angle-resolved spectra were analysed for each emitter case (O, 3F, 2C, and 1C) for randomly oriented molecules. We use the well-known parametrization[4] of the photoelectron angular distributions induced by circularly polarized light with positive and negative helicities:

$$I_{\pm 1}(\theta) = 1 \pm \beta_1 P_1(\cos\theta) - \tfrac{1}{2}\beta_2 P_2(\cos\theta) \qquad (1)$$

where β_1 and β_2 are the dichroic and anisotropy parameters, respectively, P_1 and P_2 are the first and second Legendre polynomials, and θ is the angle between the electron momentum vector and the photon propagation direction in the laboratory frame. We extracted β_2 from the sum of the angular distributions obtained for right and left circularly polarized light and the dichroic β_1 parameter from the normalized difference of these angular distributions:[11,12]

$$\text{PECD}(\cos\theta) = \frac{I_{+1}(\theta) - I_{-1}(\theta)}{I_{+1}(\theta) + I_{-1}(\theta)} = \frac{\beta_1 P_1(\cos\theta)}{1 - \dfrac{1}{2}\beta_2 P_2(\cos\theta)} \qquad (2)$$

The result is demonstrated in the left-hand panels (a,d,g,j) of Fig. 2 for all emitters. There, the experimental data (red circles with error bars reflecting statistical uncertainties) are displayed together with black solid curves showing the fitting results for β_2 and β_1 using eqn (2). These values of β_2 and β_1 are compared with the computed parameters in Table 1, which illustrates a strong influence of the origin of the photoelectron wave on the PECD of randomly oriented molecules.

While the computed and measured anisotropy parameters β_2 agree well for all emitters, the agreement between the respective dichroic parameters β_1 is rather poor. Possible reasons of such disagreement for the oxygen atom, where the computed and measured asymmetries have different signs, were discussed in ref. 12. For the three fluorine atoms (3F), both our theory and experiment yield the smallest chiral asymmetries among all emitter cases (yet, the theory predicts an asymmetry which is four times larger). The calculations show larger individual asymmetries for different fluorine atoms which compensate each other on average owing to different signs (see also ref. 26). For the two unresolved carbon atoms in the oxirane ring (2C), the computed and measured asymmetries have equal sign and are comparable in their magnitude (but still somewhat larger in the theory). For this kinetic energy of 11 eV, the computed dichroic parameter of the carbon atom in

This journal is © the Owner Societies 2022

Phys. Chem. Chem. Phys., 2022, **24**, 13597–13604 | **13599**

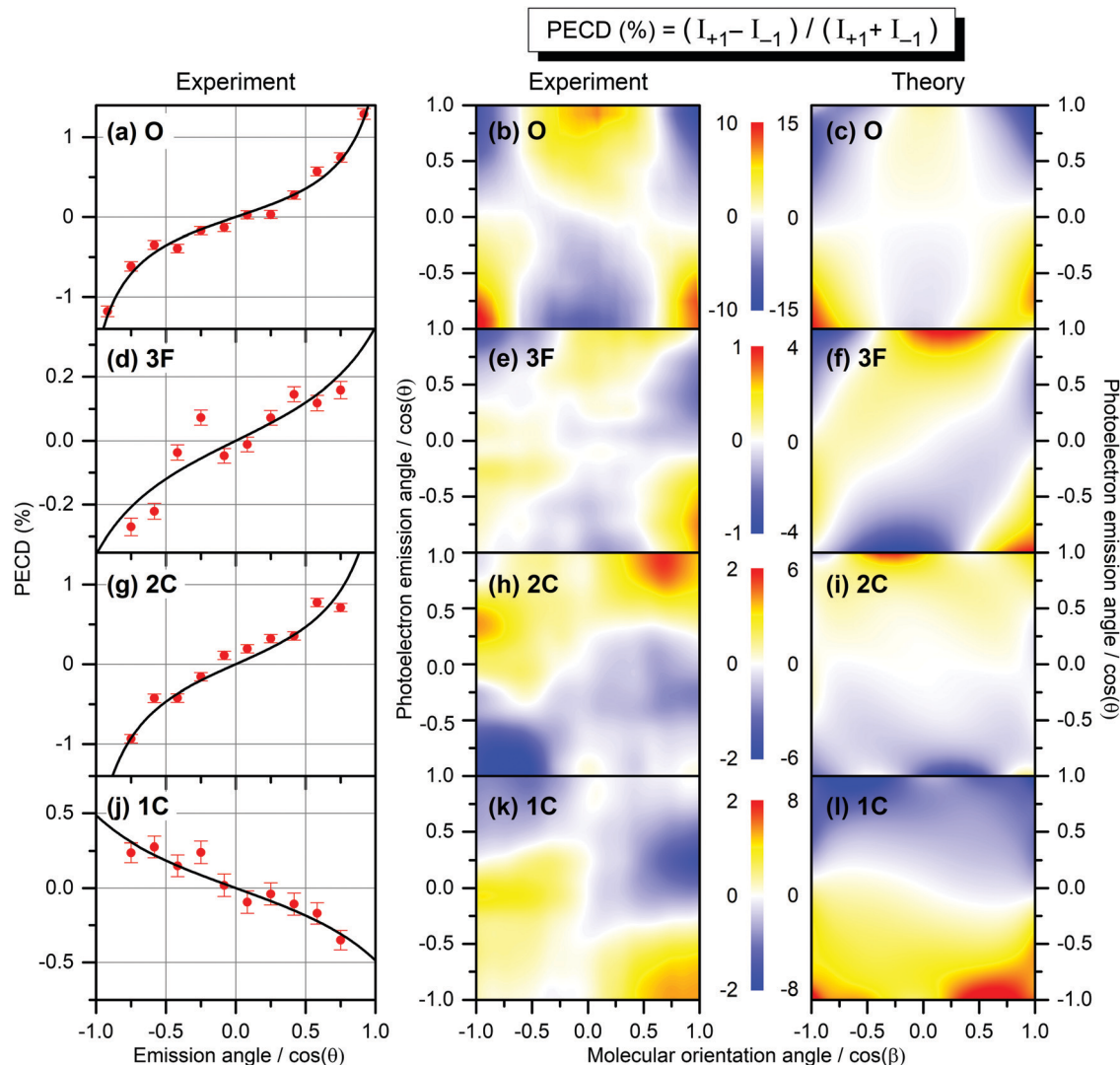$$\text{PECD (\%)} = (I_{+1} - I_{-1}) / (I_{+1} + I_{-1})$$

Fig. 2 Experimental and theoretical PECD of R-TFMOx represented as the normalized difference of the electron emission probabilities, obtained for 1s-photoelectrons of the oxygen atom (a–c, O), all three fluorine atoms (d–f, 3F), the two carbon atoms from the oxirane ring (g–i, 2C), and the carbon atom in the trifluoromethyl group (j–l, 1C). Kinetic energy of all photoelectrons is equal to about 11 eV. The left-hand panels (a,d,g,j) illustrate the retrieval of the anisotropy β_2 and dichroic β_1 parameters by fitting (black curves) the PECD, measured for randomly oriented molecules (red circles), with eqn (2). The middle and the right-hand panels illustrate the experimental (b,e,h,k) and theoretical (c,f,i,l) differential PECD as a function of the photoelectron emission angle θ and molecular orientation angle β between the momentum vector of the $CF_{2,3}^+$ fragment and the light propagation direction. The statistical uncertainties, taken at the peak values of the experimental data, are: (b, O) ±0.45%; (e, 3F) ±0.17%; (h, 2C) ±0.25%; and (k, 1C) ±0.16%.

the chiral center is +3.6% and thus larger than that of the other carbon in the oxirane ring which is −0.6%. The latter even has an opposite sign, thereby reducing the average asymmetry to +1.7%. For the carbon atom in the CF_3-group (1C), both the theory and experiment show equal sign of the asymmetry, which is opposite to that for the 2C-emitters. However, the computed asymmetry is about eight times stronger.

The influence of the origin of the photoelectron wave is even stronger if one considers the PECD of uniaxially oriented TFMOx being a two-dimensional function of the photoelectron emission angle θ and the molecular fragmentation angle β. To access this molecular fragmentation axis, the Coulomb explosion into two charged fragments was investigated, following the procedure developed in previous publications.[11,12] For

the oxygen atom, the combined fragmentation channels $CF_3^+(m/q = 69)$–$C_2H_3O^+(m/q = 43)$ and $CF_3^+(m/q = 69)$–$C_2H_2O^+(m/q = 42)$ were used in our previous work[12] to access PECD$(\cos\theta, \cos\beta)$. However, for the 3F-emitters, these two fragmentation channels are strongly suppressed (about 75% weaker as compared to the O-case). Taking into account that the 3F-, 2C-, and 1C-emitters show smaller chiral asymmetry on average than the O-emitter (see Table 1), larger statistics or, in the other words, strongly contributing fragmentation channels need to be considered to investigate PECD of uniaxially oriented TFMOx for those emitters. As was already mentioned above, the molecular-frame orientation at the instant of the photoionization and the fragment frame detected by the directions of the fragments' momentum vectors can be rather different.[43]

13600 | *Phys. Chem. Chem. Phys.*, 2022, **24**, 13597–13604

This journal is © the Owner Societies 2022

Table 1 Experimental and theoretical anisotropy β_2 and dichroic β_1 parameters of R-TFMOx at a photoelectron kinetic energy of about 11 eV. The error bars for β_1 depict the statistical errors and the standard errors of the fits only. The error bars for β_2 are based on an estimate of a systematic uncertainty due to local detector inefficiencies, which is assumed to be larger than the statistical and fit errors

Emitter atom(s)	β_2		β_1 (%)	
	Experiment	Theory	Experiment	Theory
O[a]	1.14 ± 0.15	0.86	$+0.76 \pm 0.06$	-2.9
3F	0.61 ± 0.20	0.82	$+0.25 \pm 0.05$	$+1.0$
2C	1.11 ± 0.25	0.88	$+1.00 \pm 0.10$	$+1.7$
1C	0.43 ± 0.15	0.30	-0.38 ± 0.06	-3.1

[a] Data from ref. 12.

Thus, a priori, each breakup channel and ionization site have their own fragment frame and also molecular frame at the instant of the photoionization.

In our analysis, we identified the following four incomplete fragmentation channels $CF_3^+ (m/q = 69)$–$C_2H_2^+ (m/q = 26)$, $CF_3^+ (m/q = 69)$–$COH^+ (m/q = 29)$, $CF_2^+ (m/q = 50)$–$C_2H_2^+ (m/q = 26)$, and $CF_2^+ (m/q = 50)$–$COH^+ (m/q = 29)$ as particularly suitable by matching the following four criteria: (i) they fulfill the axial-recoil approximation;[40] (ii) the reconstructed molecular axis is rather similar for all four cases; (iii) the breakup channels yield a very similar PECD($\cos\theta, \cos\beta$) pattern for the O-emitter as compared to that obtained in our previous work;[12] (iv) at least one of the breakup channels contains sufficient statistics for the further analysis. With respect to (ii), dictated by momentum conservation for complete fragmentation channels, also the angle between the momentum vectors of the two detected ions for all analysed incomplete fragmentation channels is almost $180°$ (note that neutral fragments, which are not detected in the experiment, carry only a moderate momentum and have thus very limited influence on the fragmentation axis reconstructed *via* the measured momenta of the ions). The influence of the neutral undetected particles on the fragmentation axis was estimated to introduce an uncertainty of about 13–$16°$, which is in the range of the selected data binning. Combining those four incomplete fragmentation channels for the 3F-, 2C-, and 1C-emitters results in a total increase of the statistics by a factor of about 45, as compared to the two fragmentation channels used in our previous work[12] for the O-emitter. In order to compare here PECD($\cos\theta, \cos\beta$) for different emitter sites, we reanalysed the experimental data of ref. 12 on the O-emitter, acquired for the photoelectron energy of 11 eV, using the aforementioned identified four incomplete fragmentation channels. However, employing different fragmentation channels with smaller statistics resulted in a somewhat weaker contrast of the PECD($\cos\theta, \cos\beta$) for the O-emitter ($\pm 10\%$ here as compared to $\pm 18\%$ in ref. 12), keeping the PECD landscape almost unchanged. Fig. S1 of the ESI† illustrates a satisfactorily robustness of the present analysis for all emitters with respect to the choice of only three out of the four identified channels.

The PECD($\cos\theta, \cos\beta$) maps obtained in a similar way for all emitters as described above are depicted in the middle panels (b,e,h,k) of Fig. 2. As one can see, the scales of the measured differential PECDs differ by up to an order of magnitude for the emission from different sites. The O-emitter shows by far the strongest differential PECD. Similarly to the randomly oriented samples (Table 1), the differential asymmetry is smallest for the 3F-emitters (ten times smaller than for the O-emitter), being a result of compensations of individual contributions of different signs, as already discussed in the electron-energy-dependent study of the β_1 parameter in ref. 26 (Fig. 2 there). For the O-emitter, the differential chiral asymmetry for uniaxially oriented TFMOx is about an order of magnitude larger than the average asymmetry for randomly oriented molecules (Table 1). For other emitters, however, the increase of the PECD for the uniaxially oriented molecules as compared to the randomly oriented samples is not as large, being between about 2 to 5 times. This strongly depends on the PECD landscape, *i.e.*, on its dependence on the molecular orientation angle. In particular, for the O- and 3F-emitters, the PECDs change their signs if the fragmentation axis is oriented along or perpendicularly to the light propagation direction. As a consequence, an integration over the molecular orientation reduces the effect strongly. For the 2C- and 1C-emitters, the sign of differential PECDs is almost independent of the molecular orientation angle. This results in a smaller reduction of the asymmetry on average.

The results of our calculations of the differential PECD, obtained for optimal molecular fragmentation axes, are depicted in the right-hand panels (c,f,i,l) of Fig. 2. It turns out that, for the O- and 1C-emitters, the best description of the measured PECD($\cos\theta, \cos\beta$) is provided by the fragmentation axis, which connects the CH_2-group on the oxirane ring with the oxygen atom. For the 3F-emitters, the optimal axis connects the CH_2-group and the carbon atom in the chiral center, and for the 2C-emitter the chiral center with the CF_3-group. The fact that we found notably different optimal fragmentation axes for different emitters supports our statement on the intricate fragmentation dynamics triggered by the considered K-shell photoionization of TFMOx. As one can see from Fig. 2, our theory provides a semi-quantitative description of the measured differential PECD. While the calculations reproduce the overall landscapes seen in the measured PECDs including their signs, the magnitude of the theoretical asymmetry is about 1.5 to 4 times larger for the different emitters. This can be related to the fact of using incomplete fragmentation channels, where momentum conservation was used to derive the momentum of the neutral fragment and thus cannot be used to suppress false coincidences. Furthermore, the combination of data for several channels in the experiment leads to additional averaging of the measured asymmetry. As expected, the computed PECD landscapes obey the analytically derived asymmetry rule[11] PECD($-\cos\theta, -\cos\beta$) = $-$PECD($\cos\theta, \cos\beta$), while there are noticeable deviations from this rule in the experiment indicating an insufficiency of the statistics in the acquired spectra.

4 Conclusions

We demonstrate experimentally and theoretically that the starting point of the photoelectron wave has a decisive influence on the signal strength and sign of the PECD. For this

This journal is © the Owner Societies 2022

Phys. Chem. Chem. Phys., 2022, **24**, 13597–13604 | **13601**

purpose, we examined inner-shell photoionization of different atomic species of the R-TFMOx molecule at similar photoelectron kinetic energies. In particular, we compare the PECDs obtained for the oxygen atom, the three unresolved fluorine atoms, the two unresolved carbon atoms in the oxirane ring, and the carbon atom on the trifluoromethyl group being the electron emitters. We show that the differential PECD of uniaxially oriented molecules is increased as compared to that of randomly oriented molecules. However, the signal amplification is very different for different emitters, which is dictated by the dependence of the differential PECD on the molecular orientation angle. For a practical use of PECD measurements as a tool for chiral recognition in the gas phase, thus, not only a suitable photoelectron energy should be considered, but also the orbital from which the photoelectron is ionized needs to be carefully selected to maximize the sensitivity of the method.

Author contributions

The project was supervised by R. D., P. V. D., and M. S. S. The experiment was prepared and carried out by K. F., F. T., S. G., D. T., S. E., L. B., M. H., T. J., and M. S. S. Data analysis was performed by K. F. and P. V. D. Theoretical calculations were carried out by N. M. N. and P. V. D. Initial draft was created by K. F., R. D., P. V. D., and M. S. S. All authors discussed the results and commented on the manuscript.

Conflicts of interest

There are no conflicts to declare.

Acknowledgements

References

1 A. Zehnacker, *Chiral Recognition in the Gas Phase*, CRC Press, Hoboken, 2010.

2 M. Pitzer, M. Kunitski, A. S. Johnson, T. Jahnke, H. Sann, F. Sturm, L. P. H. Schmidt, H. Schmidt-Böcking, R. Dörner, J. Stohner, J. Kiedrowski, M. Reggelin, S. Marquardt, A. Schießer, R. Berger and M. S. Schöffler, Direct Determination of Absolute Molecular Stereochemistry in Gas Phase by Coulomb Explosion Imaging, *Science*, 2013, **341**, 1096–1100.

3 M. Pitzer, *et al.*, Absolute Configuration from Different Multifragmentation Pathways in Light-Induced Coulomb Explosion Imaging, *ChemPhysChem*, 2016, **17**, 2465–2472.

4 L. Nahon, G. A. Garcia, C. J. Harding, E. Mikajlo and I. Powis, Determination of chiral asymmetries in the valence photoionization of camphor enantiomers by photoelectron imaging using tunable circularly polarized light, *J. Chem. Phys.*, 2006, **125**, 114309.

5 J. Miles, D. Fernandes, A. Young, C. M. M. Bond, S. W. Crane, O. Ghafur, D. Townsend, J. Sá and J. B. Greenwood, A new technique for probing chirality via photoelectron circular dichroism, *Anal. Chim. Acta*, 2017, **984**, 134–139.

6 M. M. R. Fanood, N. B. Ram, C. S. Lehmann, I. Powis and M. H. M. Janssen, Enantiomer-specific analysis of multi-component mixtures by correlated electron imaging–ion mass spectrometry, *Nat. Commun.*, 2015, **6**, 7511.

7 A. Comby, E. Bloch, C. M. M. Bond, D. Descamps, J. Miles, S. Petit, S. Rozen, J. B. Greenwood, V. Blanchet and Y. Mairesse, Real-time determination of enantiomeric and isomeric content using photoelectron elliptical dichroism, *Nat. Commun.*, 2018, **9**, 5212.

8 L. Nahon, L. Nag, G. A. Garcia, I. Myrgorodska, U. Meierhenrich, S. Beaulieu, V. Wanie, V. Blanchet, R. Géneaux and I. Powis, Determination of accurate electron chiral asymmetries in fenchone and camphor in the VUV range: sensitivity to isomerism and enantiomeric purity, *Phys. Chem. Chem. Phys.*, 2016, **18**, 12696–12706.

9 A. Kastner, C. Lux, T. Ring, S. Züllighoven, C. Sarpe, A. Senftleben and T. Baumert, Enantiomeric Excess Sensitivity to Below One Percent by Using Femtosecond Photoelectron Circular Dichroism, *ChemPhysChem*, 2016, **17**, 1119–1122.

10 G. A. Garcia, H. Dossmann, L. Nahon, S. Daly and I. Powis, Photoelectron circular dichroism and spectroscopy of tri-fluoromethyl- and methyl-oxirane: a comparative study, *Phys. Chem. Chem. Phys.*, 2014, **16**, 16214–16224.

11 M. Tia, *et al.*, Observation of Enhanced Chiral Asymmetries in the Inner-Shell Photoionization of Uniaxially Oriented Methyloxirane Enantiomers, *J. Phys. Chem. Lett.*, 2017, **8**, 2780–2786.

12 G. Nalin, *et al.*, Photoelectron circular dichroism of O 1s-photoelectrons of uniaxially oriented trifluoromethyloxirane: energy dependence and sensitivity to molecular configuration, *Phys. Chem. Chem. Phys.*, 2021, **23**, 17248–17258.

13 K. Fehre, *et al.*, Fourfold Differential Photoelectron Circular Dichroism, *Phys. Rev. Lett.*, 2021, **127**, 103201.

14 G. A. Garcia, H. Dossmann, L. Nahon, S. Daly and I. Powis, Identifying and Understanding Strong Vibronic Interaction Effects Observed in the Asymmetry of Chiral Molecule Photoelectron Angular Distributions, *ChemPhysChem*, 2017, **18**, 500–512.

15 G. A. Garcia, L. Nahon, S. Daly and I. Powis, Vibrationally induced inversion of photoelectron forward-backward asymmetry in chiral molecule photoionization by circularly polarized light, *Nat. Commun.*, 2013, **4**, 2132.

16 H. Ganjitabar, R. Hadidi, G. A. Garcia, L. Nahon and I. Powis, Vibrationally-resolved photoelectron spectroscopy

13602 | *Phys. Chem. Chem. Phys.*, 2022, **24**, 13597–13604

This journal is © the Owner Societies 2022

and photoelectron circular dichroism of bicyclic monoterpene enantiomers, *J. Mol. Spectrosc.*, 2018, **353**, 11–19.

17 D. Di Tommaso, M. Stener, G. Fronzoni and P. Decleva, Conformational Effects on Circular Dichroism in the Photoelectron Angular Distribution, *ChemPhysChem*, 2006, **7**, 924–934.

18 S. Turchini, D. Catone, N. Zema, G. Contini, T. Prosperi, P. Decleva, M. Stener, F. Rondino, S. Piccirillo, K. C. Prince and M. Speranza, Conformational Sensitivity in Photoelectron Circular Dichroism of 3-Methylcyclopentanone, *ChemPhysChem*, 2013, **14**, 1723–1732.

19 S. Turchini, Conformational effects in photoelectron circular dichroism, *J. Phys.: Condens. Matter*, 2017, **29**, 503001.

20 L. Nahon, G. A. Garcia, H. Soldi-Lose, S. Daly and I. Powis, Effects of dimerization on the photoelectron angular distribution parameters from chiral camphor enantiomers obtained with circularly polarized vacuum-ultraviolet radiation, *Phys. Rev. A*, 2010, **82**, 032514.

21 S. Beaulieu, A. Comby, D. Descamps, B. Fabre, G. A. Garcia, R. Géneaux, A. G. Harvey, F. Légaré, Z. Mašín, L. Nahon, A. F. Ordonez, S. Petit, B. Pons, Y. Mairesse, O. Smirnova and V. Blanchet, Photoexcitation circular dichroism in chiral molecules, *Nat. Phys.*, 2018, **14**, 484–489.

22 A. Comby, S. Beaulieu, M. Boggio-Pasqua, D. Descamps, F. Légaré, L. Nahon, S. Petit, B. Pons, B. Fabre, Y. Mairesse and V. Blanchet, Relaxation Dynamics in Photoexcited Chiral Molecules Studied by Time-Resolved Photoelectron Circular Dichroism: Toward Chiral Femtochemistry, *J. Phys. Chem. Lett.*, 2016, **7**, 4514–4519.

23 S. Beaulieu, A. Comby, B. Fabre, D. Descamps, A. Ferré, G. Garcia, R. Géneaux, F. Légaré, L. Nahon, S. Petit, T. Ruchon, B. Pons, V. Blanchet and Y. Mairesse, Probing ultrafast dynamics of chiral molecules using time-resolved photoelectron circular dichroism, *Faraday Discuss.*, 2016, **194**, 325–348.

24 K. Fehre, S. Eckart, M. Kunitski, C. Janke, D. Trabert, M. Hofmann, J. Rist, M. Weller, A. Hartung, L. P. H. Schmidt, T. Jahnke, H. Braun, T. Baumert, J. Stohner, P. V. Demekhin, M. S. Schöffler and R. Dörner, Strong Differential Photoion Circular Dichroism in Strong-Field Ionization of Chiral Molecules, *Phys. Rev. Lett.*, 2021, **126**, 083201.

25 M. Stener, G. Fronzoni, D. Di Tommaso and P. Decleva, Density functional study on the circular dichroism of photoelectron angular distribution from chiral derivatives of oxirane, *J. Chem. Phys.*, 2004, **120**, 3284.

26 M. Ilchen, G. Hartmann, P. Rupprecht, A. N. Artemyev, R. N. Coffee, Z. Li, H. Ohldag, H. Ogasawara, T. Osipov, D. Ray, P. Schmidt, T. J. A. Wolf, A. Ehresmann, S. Moeller, A. Knie and P. V. Demekhin, Emitter-site-selective photoelectron circular dichroism of trifluoromethyloxirane, *Phys. Rev. A*, 2017, **95**, 053423.

27 M. M. Rafiee Fanood, M. H. M. Janssen and I. Powis, Wavelength dependent photoelectron circular dichroism of limonene studied by femtosecond multiphoton laser ionization and electron-ion coincidence imaging, *J. Chem. Phys.*, 2016, **145**, 124320.

28 A. Kastner, T. Ring, B. C. Krüger, G. B. Park, T. Schäfer, A. Senftleben and T. Baumert, Intermediate state dependence of the photoelectron circular dichroism of fenchone observed via femtosecond resonance-enhanced multi-photon ionization, *J. Chem. Phys.*, 2017, **147**, 013926.

29 D. Catone, M. Stener, P. Decleva, G. Contini, N. Zema, T. Prosperi, V. Feyer, K. C. Prince and S. Turchini, Resonant Circular Dichroism of Chiral Metal-Organic Complex, *Phys. Rev. Lett.*, 2012, **108**, 083001.

30 G. Hartmann, M. Ilchen, P. Schmidt, C. Küstner-Wetekam, C. Ozga, F. Scholz, J. Buck, F. Trinter, J. Viefhaus, A. Ehresmann, M. S. Schöffler, A. Knie and P. V. Demekhin, Recovery of High-Energy Photoelectron Circular Dichroism through Fano Interference, *Phys. Rev. Lett.*, 2019, **123**, 043202.

31 N. Böwering, T. Lischke, B. Schmidtke, N. Müller, T. Khalil and U. Heinzmann, Asymmetry in Photoelectron Emission from Chiral Molecules Induced by Circularly Polarized Light, *Phys. Rev. Lett.*, 2001, **86**, 1187.

32 I. Powis, C. J. Harding, S. Barth, S. Joshi, V. Ulrich and U. Hergenhahn, Chiral asymmetry in the angle-resolved O and C $1s^{-1}$ core photoemissions of the R enantiomer of glycidol, *Phys. Rev. A*, 2008, **78**, 052501.

33 J. Viefhaus, F. Scholz, S. Deinert, L. Glaser, M. Ilchen, J. Seltmann, P. Walter and F. Siewert, The Variable Polarization XUV Beamline P04 at PETRA III: Optics, mechanics and their performance, *Nucl. Instrum. Methods Phys. Res., Sect. A*, 2013, **710**, 151–154.

34 K. Fehre, M. Pitzer, F. Trinter, R. Berger, A. Schießer, H. Schmidt-Böcking, R. Dörner and M. S. Schöffler, Closed-loop recycling of rare liquid samples for gas-phase experiments, *Rev. Sci. Instrum.*, 2021, **92**, 023205.

35 R. Dörner, V. Mergel, O. Jagutzki, L. Spielberger, J. Ullrich, R. Moshammer and H. Schmidt-Böcking, Cold Target Recoil Ion Momentum Spectroscopy: a 'momentum microscope' to view atomic collision dynamics, *Phys. Rep.*, 2000, **330**, 95–192.

36 J. Ullrich, R. Moshammer, A. Dorn, R. Dörner, L. P. H. Schmidt and H. Schmidt-Böcking, Recoil-ion and electron momentum spectroscopy: reaction-microscopes, *Rep. Prog. Phys.*, 2003, **66**, 1463.

37 T. Jahnke, T. Weber, T. Osipov, A. L. Landers, O. Jagutzki, L. P. H. Schmidt, C. L. Cocke, M. H. Prior, H. Schmidt-Böcking and R. Dörner, Multicoincidence studies of photo and Auger electrons from fixed-in-space molecules using the COLTRIMS technique, *J. Electron Spectrosc. Relat. Phenom.*, 2004, **141**, 229–238.

38 W. C. Wiley and I. H. McLaren, Time-of-Flight Mass Spectrometer with Improved Resolution, *Rev. Sci. Instrum.*, 1955, **26**, 1150.

39 K. Fehre, D. Trojanowskaja, J. Gatzke, M. Kunitski, F. Trinter, S. Zeller, L. P. H. Schmidt, J. Stohner, R. Berger, A. Czasch, O. Jagutzki, T. Jahnke, R. Dörner and M. S. Schöffler, Absolute ion detection efficiencies of microchannel plates and funnel microchannel plates for multi-coincidence detection, *Rev. Sci. Instrum.*, 2018, **89**, 045112.

40 R. N. Zare, Photoejection dynamics, *Mol. Photochem.*, 1972, **4**, 1–37.

41 P. V. Demekhin, A. Ehresmann and V. L. Sukhorukov, Single center method: A computational tool for ionization and

This journal is © the Owner Societies 2022

Phys. Chem. Chem. Phys., 2022, **24**, 13597–13604 | **13603**

electronic excitation studies of molecules, *J. Chem. Phys.*, 2011, **134**, 024113.

42 S. A. Galitskiy, A. N. Artemyev, K. Jänkälä, B. M. Lagutin and P. V. Demekhin, Hartree-Fock calculation of the differential photoionization cross sections of small Li clusters, *J. Chem. Phys.*, 2015, **142**, 034306.

43 K. Fehre *et al.*, *Enantiosensitive Structure Determination by Photoelectron Scattering on Single Molecules*, arXiv:2101.03375.

13604 | *Phys. Chem. Chem. Phys.*, 2022, **24**, 13597–13604

This journal is © the Owner Societies 2022